Title

Developmental trajectories of cerebral blood flow and oxidative metabolism at baseline and during working memory tasks.

Authors

Jog, Mayank A
Yan, Lirong
Kilroy, Emily
et al.

Publication Date

2016-07-01

DOI

10.1016/j.neuroimage.2016.04.035

Peer reviewed

NeuroImage 134 (2016) 587–596

Contents lists available at ScienceDirect

NeuroImage

journal homepage: www.elsevier.com/locate/ynimg

Developmental trajectories of cerebral blood flow and oxidative metabolism at baseline and during working memory tasks

Mayank A. Jog [a,1], Lirong Yan [a,1], Emily Kilroy [a], Kate Krasileva [a], Kay Jann [a], Holly LeClair [b], David Elashoff [b], Danny J.J. Wang [a,*]

[a] Laboratory of FMRI Technology (LOFT), Department of Neurology, University of California Los Angeles, Los Angeles, CA, USA
[b] Department of Medicine Statistics Core, UCLA, Los Angeles, CA, USA

ARTICLE INFO

Article history:
Received 17 October 2015
Revised 11 April 2016
Accepted 14 April 2016
Available online 18 April 2016

Keywords:
Developmental fMRI
Working memory
Cerebral blood flow (CBF)
Cerebral metabolic rate of oxygen consumption ($CMRO_2$)
Neurovascular coupling

ABSTRACT

The neurobiological interpretation of developmental BOLD fMRI findings remains difficult due to the confounding issues of potentially varied baseline of brain function and varied strength of neurovascular coupling across age groups. The central theme of the present research is to study the development of brain function and neuronal activity through in vivo assessments of cerebral blood flow (CBF), oxygen extraction fraction (OEF) and cerebral metabolic rate of oxygen ($CMRO_2$) both at baseline and during the performance of a working memory task in a cohort of typically developing children aged 7 to 18 years. Using a suite of 4 emerging MRI technologies including MR blood oximetry, phase-contrast MRI, pseudo-continuous arterial spin labeling (pCASL) perfusion MRI and concurrent CBF/BOLD fMRI, we found: 1) At baseline, both global CBF and $CMRO_2$ showed an age related decline while global OEF was stable across the age group; 2) During the working memory task, neither BOLD nor CBF responses showed significant variations with age in the activated fronto-parietal brain regions. Nevertheless, detailed voxel-wise analyses revealed sub-regions within the activated fronto-parietal regions that show significant decline of fractional $CMRO_2$ responses with age. These findings suggest that the brain may become more "energy efficient" with age during development.

1. Introduction

Although the development of a human brain is influenced by genetic and environmental factors, neuroimaging studies in the past few decades have revealed systematic population-wide patterns for the maturation of brain structure and function. For instance, the developmental trajectory of cortical and subcortical gray matter follows an inverted U-shaped function whereas the volume and anisotropy of white matter fiber bundles generally increase with age, following a region-specific fashion (Giedd et al., 1999; Gogtay et al., 2004; Lenroot and Giedd, 2006).

Functional MRI(fMRI) using the blood oxygen level dependent (BOLD) contrast (Kwong et al., 1992; Ogawa et al., 1990) has been widely applied for studying the development of language, emotion, executive, and memory functions in children and adolescents (Casey et al., 2005; Paus, 2005). In general, developmental BOLD fMRI studies using spatial and verbal working memory tasks have reported increased BOLD signal changes with age in executive brain networks involving fronto-parietal regions (Klingberg et al., 2002a; Kwon et al., 2002; Thomason et al., 2009). These findings were interpreted as increased neuronal activity within the executive networks with brain maturation. However, other working memory fMRI studies have reported either a stable BOLD activation pattern across age groups (Thomas et al., 1999) or increased recruitment of fronto-parietal brain regions with age (Crone et al., 2006). In addition, an fMRI study of children employing an inhibition control (Go/No Go) task (Tamm et al., 2002) reported both increased and decreased BOLD activations with age in different regions within the prefrontal cortex. Because the signal strength of BOLD fMRI is intrinsically tied to the strength of the neurovascular coupling which may vary across the population (Harris et al., 2011), there remains a large gap between the observed developmental trends in BOLD fMRI and the underlying changes of neuronal function.

Emerging studies have applied noninvasive arterial spin labeling (ASL) perfusion MRI techniques to understand the development of brain function through a surrogate marker – cerebral blood flow (CBF) (Taki et al., 2011a, 2011b; Wang and Licht, 2006). It has been shown that CBF is more closely related to neuronal activities through neurovascular coupling compared to BOLD signals (Chen et al., 2015). With careful adjustment of age related changes in gray matter volume and physiological parameters (Jain et al., 2012), region and sex-specific growth curves of CBF that diverge between the two sexes around puberty (Satterthwaite et al., 2014) have been observed. However, relating developmental CBF findings to the maturation of neuronal

* Corresponding author at: Department of Neurology, University of California Los Angeles, 660 Charles E Young Dr South, Los Angeles, CA 90095, USA.
E-mail address: jwang71@gmail.com (D.J.J. Wang).
[1] These two authors contribute equally to the study.

http://dx.doi.org/10.1016/j.neuroimage.2016.04.035
1053-8119/

function may still be confounded by nonspecific vascular effects and subject to the strength of neurovascular coupling across developing populations (Leithner and Royl, 2014).

A potentially more accurate index of neuronal function is cerebral metabolic rate of oxygen consumption ($CMRO_2$). Recent advances in neuroenergetics (Belanger et al., 2011) indicate that neuronal demand is the principal driver of changes in oxygen consumption while the metabolic profile of astrocytes remains largely glycolytic. In addition, electrophysiological studies performed in rat brains (Hyder et al., 2002; Maandag et al., 2007) reported that fractional changes in $CMRO_2$ during forepaw stimulation were approximately equal to measured fractional changes in neuronal firing rate. To date, however, very few studies have investigated the evolution of $CMRO_2$ during brain development.

The central theme of the present research is to study the development of brain function and neuronal metabolism through in vivo assessments of CBF, OEF and $CMRO_2$ both at baseline and during the performance of a working memory task in a cohort of typically developing children aged 7 to 18 years. To this end, we developed and adapted a suite of MRI techniques for in vivo assessment of CBF, oxygen extraction fraction (OEF) and subsequently $CMRO_2$, including: 1) MR blood oximetry that exploits the intrinsic susceptibility of deoxygenated hemoglobin (Jain et al., 2010); 2) Phase-contrast (PC) MRI that measures the average blood inflow rate to the brain (Jain et al., 2012); 3) Pseudo-continuous ASL (pCASL) for CBF measurement by utilizing magnetically labeled arterial blood water as an endogenous tracer (Wang and Licht, 2006); and 4) Concurrent CBF/BOLD fMRI using dual-echo echo-planar imaging (DE-EPI) pCASL. The combination of the four quantitative MRI techniques is expected to offer comprehensive in vivo assessments of both global and regional oxidative metabolism at baseline and during working memory tasks through childhood and adolescence.

2. Methods

2.1. Participants

Healthy, typically-developing children between 7 and 18 years of age were enrolled in the NIMH funded study entitled "Pediatric Template of Brain Perfusion" (Avants et al., 2015). Phone interviews were conducted to exclude subjects who had any history of neurologic or psychiatric disorders, abuse of drugs or alcohol, major systemic diseases, or contraindications to MRI. Written informed consent was obtained from each subject and his or her parents according to a protocol approved by the Institutional Review Board (IRB) of the University of California, Los Angeles (UCLA). Here we report results from 91 typically developing children aged 7 to 18 years (44 male, age = 13.5 ± 2.7 yr). The mean Full Scale IQ of the enrolled cohort was 107.6 ± 16.4 which did not show significant variation with age.

2.2. MRI experiment

All MRI data were acquired on a Siemens TIM Trio 3T MR system using the product 12-channel head coil. All participants underwent resting state PC MRI, blood oximetry and pCASL scans, as well as concurrent CBF/BOLD fMRI of working memory tasks. Fig. 1 displays the experimental paradigm and associated imaging sequences and analyses.

2.2.1. Resting-state global CBF, OEF and CMRO2 assessment

Phase-contrast (PC) MRI (VENC = 80 cm/s; TE/TR = 5.23/18 ms; FOV = 200 × 200 mm^2; matrix = 192 × 192; slice thickness = 5 mm, scan time = 1 min) was acquired at the level of the mouth (between C1 and C2 vertebrae) to quantify mean flow velocities in internal carotid and vertebral arteries (Jain et al., 2012). Total cerebral blood flow volume (CBFV) was calculated as

$$\mathrm{CBFV} = \sum_{\mathrm{Voxels}} \left[\left(\frac{\Delta\Phi \times \mathrm{VENC}}{\pi} \right) \times A_{\mathrm{Voxel}} \right] \quad (1)$$

where A_{Voxel} is the cross sectional area of the arteries, $\Delta\Phi$ is the measured phase in PC MRI, VENC is the encoding velocity. CBF was estimated by dividing CBFV with the brain mass estimated from the product of brain volume (estimated from T1 weighted structural MRI after skull striping in each individual subject) and density (Jain et al., 2010).

Susceptibility based MRI blood oximetry was acquired using a magnetic field mapping sequence (TE_1 = 5.18 ms; TE_2 = 7.64 ms; TR = 100 ms; FOV = 200 × 200 mm^2; matrix = 192 × 192; slice

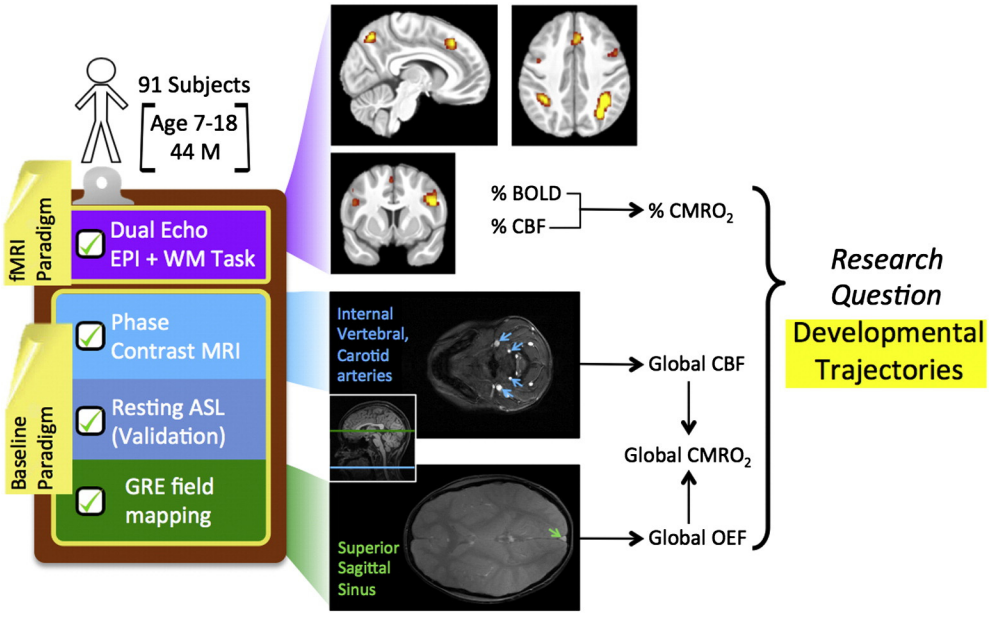

Fig. 1. Illustration of the experimental paradigm and imaging sequences applied in the present study, along with corresponding physiological parameters assessed by these techniques. Group-level activation maps of BOLD and CBF were obtained from concurrent ASL/BOLD data. Percentage BOLD and CBF signal changes were calculated from the ROIs of conjunction analyses. Percentage $CMRO_2$ changes in response to WM tasks were subsequently estimated based on the Davis Model. Global CBF and OEF were calculated from PC-MRI and GRE field mapping, respectively. Baseline regional CBF was assessed by a pCASL EPI scan. Baseline $CMRO_2$ was then calculated using quantified CBF and OEF according to Fick's principle.

thickness = 5 mm, scan time = 1 min) applied at an axial plane perpendicular to the superior sagittal sinus (SSS). The venous oxygen saturation fraction, SvO_2, was estimated by

$$SvO_2 = 1 - \frac{2|\Delta\Phi|}{Hct \times \gamma B_0 (\cos^2\theta - 1/3) \times \Delta\chi_{do}} \quad (2)$$

where $\Delta\Phi$ is the phase difference between the venous blood in SSS and surrounding tissue, *Hct* is hematocrit, B_0 is the static magnetic field of the MRI, θ is the angle between vessel and B_0, $\Delta\chi_{do} = 4\pi \cdot 0.27$ ppm. and γ is the gyromagnetic ratio (Jain et al., 2010). The arterial oxygen saturation fraction, SaO_2, was assumed to be 98%. $CMRO_2$ was then calculated using quantified CBF and OEF, according to Fick's principle

$$CMRO_2 = C_a CBF(SaO_2 - SvO_2) \quad (3)$$

where Ca is the blood's oxygen carrying capacity. For calculations of both Eqs. (2) and (3), we carefully adjusted the developmental changes in *Hct* and Ca based on literature values in children (Wu et al., 2010) (see Supplement Fig. S1).

In addition, a pseudo-continuous ASL (pCASL) sequence with 2D EPI readout (TR/TE = 4000/11 ms, FOV = 22 cm, matrix = 64 × 64, 24 × 5 mm slices with 1 mm gap, post-labeling delay (PLD) = 1.2 s, labeling duration = 1.5 s, labeling offset = 9 cm, 80 acquisitions with a scan time of 5 min) was applied to map regional CBF in the same developing cohort, which was calculated using a published model with age and gender dependent blood T1 values (Jain et al., 2012). During all resting scans, subjects were instructed to look at a fixation cross on a black screen while keeping their heads still.

2.2.2. Concurrent CBF and BOLD fMRI of working memory tasks

A dual-echo EPI pCASL scan was performed for concurrent CBF and BOLD fMRI. Imaging parameters were: FOV = 220 mm, matrix size = 64 × 64, TE_1/TE_2 = 10/25 ms, TR = 3.5 s, rate-2 GRAPPA, 7/8 partial k-space, 20 slices with 5 mm thickness and 1 mm gap, 140 acquisitions with a scan time of 8 min 10 s. The tagging plane was positioned 90 mm inferior to the center of the imaging slab with a labeling duration of 1500 ms and PLD of 1000 ms. MRI compatible video goggles were used to display the stimuli and participants were provided with a button box to record task-responses.

A 2-back verbal working memory (WM) task was employed for concurrent CBF/BOLD fMRI. Compared to visuospatial working memory tasks, language functions have been shown to mature at a relatively early developmental stage with reliable fMRI activation patterns from childhood through adolescence (Szaflarski et al., 2012). A block design fMRI paradigm was employed with 5 cycles of interleaved 34 s 0-back and 64 s 2-back tasks. Subjects were required to monitor a visually presented random sequence of letters, and press a button every time a target letter was displayed on the screen. For the 0-back task (control condition), the target letter was an "x", while it was a sequence of sandwiched letters for the 2-back condition (e.g. "A–B–A", Stimulus present time = 1.5 s, Inter-stimulus duration = 0.5 s). Each subject underwent a practice session before the MRI experiment, during which they became familiar with the tasks until their performance stabilized. At the beginning of the fMRI scan, a 15 s brief instruction was shown on the screen.

2.2.3. $CMRO_2$ estimation of concurrent ASL/BOLD fMRI

$CMRO_2$ changes in response to working memory tasks were estimated according to the Davis Model (Davis et al., 1998),

$$fCMRO_2 = \left[\frac{\left(1 - \frac{fBOLD}{M}\right)^{\frac{1}{\beta}}}{(1 + fCBF)^{\left(\frac{\alpha}{\beta} - 1\right)}}\right] - 1 \quad (4)$$

where *f*BOLD and *f*CBF are the fractional changes in BOLD and CBF data respectively, and $\alpha = 0.2, \beta = 1.3$ (Chen and Pike, 2009). The calibration constant *M* is usually estimated using a hypercapnia experiment which is not feasible in our pediatric population. We assumed *M* of 0.07 based on reported literature values (Davis et al., 1998; Lu et al., 2011). Additionally, potential variations in *M* with age were estimated using two models incorporating whole brain resting CBF, OEF and $CMRO_2$ measurements in the present study and *Hct* values from literature (Wu et al., 2010):

Model 1 (Hoge et al., 1999):

$$M = TE \cdot B \cdot CBF_0^{\alpha} \cdot \left[\frac{1}{4} \cdot \frac{CMRO2_0}{CBF_0}\right]^{\beta} \quad (5)$$

Model 2 (Davis et al., 1998; Lu et al., 2011):

$$M = TE \cdot A \cdot CBF_0^{\alpha} \cdot [Hct \cdot (1 - SvO_2)]^{\beta} \quad (6)$$

Here, CBF_0 is the baseline global CBF; $CMRO2_0$ is the baseline global $CMRO_2$; TE, A and B are constants related to imaging parameters and magnetic field strength. While no significant variation in *M* with age was observed with Model 1, Model 2 predicted a 10% increase in *M* with age ($p = 0.96$ and 2.4×10^{-5} respectively, see Supplementary Fig. S2). In summary, two models of *M* variation with age were employed to calculate $CMRO_2$ for subsequent analyses:

M1: $M = 0.07$ for every participant;

M2: *M* varies linearly: −5% to +5% of .07 across the age range of 7–18 years.

With each of the 2 models, we calculated voxel-wise *f*$CMRO_2$ changes in response to working memory tasks.

2.2.4. OEF Estimation

Eq. (3) can be reformulated to express the fractional change in OEF in terms of the fractional changes in CBF and $CMRO_2$ as

$$fOEF = \frac{fCMRO_2 - fCBF}{1 + fCBF}. \quad (7)$$

Therefore, the calculated *f*$CMRO_2$ and *f*CBF values can be used to estimate *f*OEF.

2.3. Data analysis

2.3.1. Global baseline measurement of CBF, OEF and $CMRO_2$

All post-processing was performed using custom programs in MATLAB R2011a. Global CBF, OEF and $CMRO_2$ were calculated from PC-MRI and blood oximetry maps using a custom program. For PC-MRI, the cross-sectional area of arteries was defined by thresholding on complex subtracted magnitude images. Pearson correlation coefficients were calculated between all three parameters (global CBF, OEF and $CMRO_2$) and age, with gray and white matter volume fraction (see below) included as covariates. Global CBF values estimated using PC-MRI and resting pCASL scans were correlated.

2.3.2. Working Memory fMRI with Concurrent CBF and BOLD

Behavioral performance was evaluated using D-prime defined as $D' = Z(H) - Z(F)$ where z(H) and z(F) are the z transforms of hit rate and false alarm, respectively (Wickens, 2001). All fMRI data were processed using SMP8 and custom Matlab programs. For the first and second echo pCASL EPI data, rigid head motion correction was performed on the label and control image series respectively. Participants with excessive motion (Translational Displacement > 3.4 mm (one voxel), or Rotational Displacement > 2°) were excluded resulting in a total of 91 participants. The degree of head motion was compared across subjects by calculating the mean Framewise Displacement (FD) (Power et al., 2012). Using the first echo time-series, a perfusion-weighted time-series was generated by pairwise

sinc-subtraction of control and label images. Quantitative CBF were calculated using a standard model taking into account age and gender dependent blood T1 changes (Jain et al., 2012), while assuming a labeling efficiency of 0.85. PCASL images were coregistered to the brain-extracted structural T1 MPRAGE scan in each individual subjects, followed by normalization to the study specific pediatric template in the MNI space constructed using the Advanced Normalization Tools (ANTs)(Avants et al., 2015). Images were subsequently spatially smoothed using a Gaussian kernel (FWHM: $8 \times 8 \times 8$ mm).

A general linear model (GLM) regression analysis was performed on the second echo pCASL data (TE2 = 25 ms) to derive BOLD activation with the following regressors: 1) a task regressor of 2- and 0-back conditions convolved with a double-gamma hemodynamic response function; and 2) an ASL signal regressor (alternating values of 0.5, −0.5 for control, tag respectively). To derive ASL activation, regression analysis was performed on calculated CBF time series based on the first echo pCASL data (TE1 = 10 ms). Second-level group analysis of 2-back relative to 0-back WM was performed using one-sample t-test to obtain the activation map of BOLD and ASL fMRI across the age group respectively. Statistical maps were thresholded to display group activation maps for BOLD (Family-wise error (FWE) corrected $p < 0.05$, cluster size > 100) and CBF data (False discovery rate (FDR) corrected $p < 0.05$; cluster size > 100) respectively.

2.3.3. $CMRO_2$ estimation

A conjunction analysis was performed to determine the commonly activated ROIs for CBF and BOLD fMRI. First, group-level BOLD activation maps were thresholded at FWE corrected significance of $p < 0.05$, which were applied on the CBF data to obtain group level CBF activation at FDR corrected $p < 0.05$ level. This conjunction analysis identified 6 ROIs (listed in Table 1) within the fronto-parietal executive network. In the common ROIs, voxelwise absolute and %CBF as well as %BOLD signal changes between 2-back and 0-back conditions were calculated, and %$CMRO_2$ change was estimated according to Eq. (4) using each of the 2 models of M variation with age respectively. For regression analyses of functional signal changes as a function of age, signal changes in $CMRO_2$, BOLD, CBF and OEF were regressed with age.

Table 1
Details of each activation cluster from BOLD, ASL, and conjunction analysis including anatomical locations, cluster size, coordinates and T value of the peak.

Anatomical locations	Cluster size	Peak coordinate	Peak value (T)
BOLD FWE $p < 0.05$, Cluster size > 100			
R.IFG/Insula	384	32 24 −4	10.0839
R. Middle frontal gyrus/DLPFC(BA 9/46)/precentral	4049	30 8 58	11.0826
L. Caudate	185	−16 2 18	6.5628
L. Middle frontal gyrus/precentral/L. IFG (44/45)/DLPFC(9/46)	3628	−46 8 24	9.5005
Bilateral parietal	8012	36 −52 46	13.9629
Medial frontal gyrus/SMA/cingulate gyrus	1556	2 24 44	9.6578
ASL FDR $p < 0.05$, Cluster size > 100			
L. Middle frontal gyrus/L. precentral	236	−48 2 44	6.2892
	107	−32 2 60	5.8652
R. IFG	602	48 10 28	6.5204
Dorsal ACC/SMA	491	4 28 44	6.3695
L. Inferior parietal lobe	605	−38 −44 44	6.6703
R. Inferior parietal lobe	1467	38–50 42	8.2778
Precuneus	224	6 −66 50	6.8837
Conjunction, FDR $p < 0.05$			
L. Precentral/L. middle frontal gyrus/L. IFG	193	−48 2 44	6.2892
R. Middle frontal gyrus/R. IFG/R. DLPFC(9/46)	409	48 10 28	6.5204
Dorsal ACC/SMA	443	4 28 44	6.3695
L. Inferior parietal	553	−38 −44 44	6.6703
R. Inferior parietal	1389	38 −50 42	8.2778
Precuneus	181	6 −66 50	6.8837

Abbreviations: IFG, inferior frontal gyrus; DLPFC, dorsolateral prefrontal cortex; ACC, anterior cingulate cortex; SMA, supplementary motor area.

2.3.4. Sub-regional voxel-wise analysis

Since brain regions with $CMRO_2$ changes – theoretically linked to neuronal activity changes – may only constitute sub-regions or "hubs" within BOLD and CBF activation ROIs, estimation of fractional $CMRO_2$ changes during working memory tasks were carried out across voxels within the activation ROIs. (Spearman) Correlation coefficients of $f$$CMRO_2$ vs. age were calculated on a voxel level to identify sub-regions with significant variations with age. The results were corrected for multiple comparisons using small volume cluster correction (implemented using AlphaSim (Song et al., 2011)). To concisely visualize the reliability of significant sub-regions identified using the two M models, Dice similarity coefficient (DC) was calculated, according to

$$DC = \frac{2|A \cap B|}{|A| + |B|} \tag{8}$$

where A and B indicate the respective activation clusters.

3. Results

3.1. Developmental trajectories of global CBF, OEF and $CMRO_2$ at baseline

Global OEF estimated by MRI blood oximetry did not show significant variation with age ($R = -0.019$, $p = 0.86$, Fig. 2A). Global CBF estimated using PC MRI decreased with age ($R = -0.38$, $p = 0.0005$, Fig. 2B), which was also positively correlated with global CBF estimated using pCASL ($R = 0.46$, $p = 0.000015$, Fig. 2D). Global $CMRO_2$ decreased with age ($R = -0.28$, $p = 0.00096$, Fig. 2C). The above developmental trends were similarly observed for male and female children, and were present after adjusting changes in the gray and white matter volume with age (OEF vs. age: $R = 0.041$, $p = 0.70$; CBF using PC-MRI vs. age: $R = -0.46$, $p = 0.000017$ $CMRO_2$ vs. age: $R = -0.25$, $p = 0.022$).

3.2. Developmental trajectories of CBF and $CMRO_2$ during working memory tasks

The behavioral performance (D′) of the subjects for the 2-back WM task was 4.24 ± 0.75 which increased significantly with age ($R = 0.34$, $p = 0.002$)(Fig. 3). No significant variation in the degree of head motion indicated by mean FD with age was observed ($p = 0.18$, slope = −0.01 mm/years). Fig. 4 shows group level activation maps of 2-back vs. 0-back contrast for BOLD and CBF data respectively, corrected for multiple comparisons. Reliable brain activations associated with 2-back relative to 0-back WM task were observed in bilateral prefrontal, parietal cortex and anterior cingulate cortex (ACC) in BOLD and ASL data. As expected, BOLD data yielded stronger task-induced brain activation than ASL. The conjunction analyses of ASL and BOLD activations identified 6 ROIs, as listed in Table 1, including left precentral/left middle frontal gyrus/left inferior frontal gyrus, right middle frontal gyrus/right inferior frontal gyrus/right dorsolateral prefrontal cortex (Brodmann area 9/46), dorsal anterior cingulate cortex/supplementary motor area, left inferior parietal, right inferior parietal, and precuneus. An integrated ROI was generated by combining all 6 ROIs. Table 1 lists the activation clusters detected in ASL and BOLD fMRI respectively.

3.3. ROI analyses

The percentage BOLD signal change between 2 and 0-back WM tasks as a function of age in the combined ROI is shown in Fig. 5A, which did not show significant variation with age. Compared to BOLD, ASL was able to provide task-induced CBF changes both in absolute unit (ml/

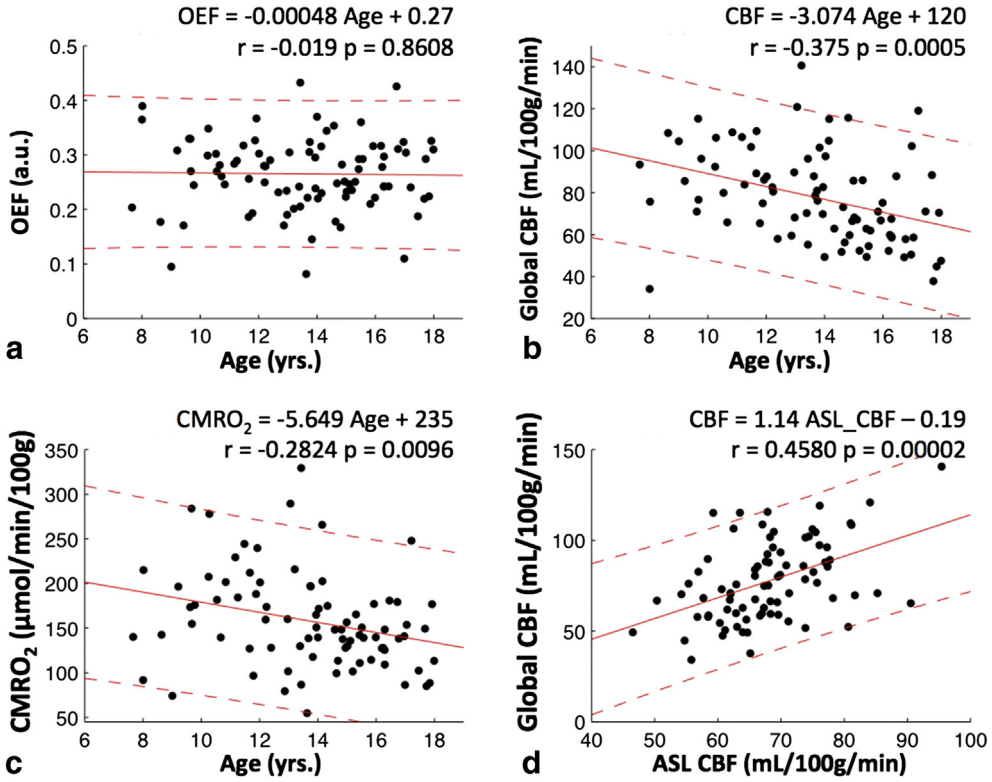

Fig. 2. Developmental changes in global OEF (a), CBF (b) and $CMRO_2$ (c) at baseline. The correlation between global CBF values estimated by PC-MRI and pCASL scans is shown (d). Dashed lines indicate 95% confidence interval.

100 g/min) and fractional signal changes (%). Fig. 5B and C show the scatter plots of mean fractional and absolute CBF change (ΔCBF) with age within the combined ROI, respectively. Both the task-induced absolute and percentage CBF changes did not show variations with age. As a result, the estimated fractional changes in $CMRO_2$ during 2-back WM relative to 0-back WM task did not vary significantly with age (Fig. 4D), using either model M1 or M2. Performing the above regression analyses for each of the 6 ROIs individually did not reveal significant variations of task-induced BOLD, CBF or $CMRO_2$ changes with age.

3.4. Voxel-wise analysis within activated ROIs

Within the commonly activated ROIs of BOLD and CBF data, a voxel-wise regression analysis was performed on fractional changes in $CMRO_2$ with age. We found significant negative correlations between $CMRO_2$ changes and age in 2 sub-regions within the left precentral/IFG, and right MFG/IFG/DLPFC areas (cluster corrected $p < 0.05$) using both M models, as illustrated in Fig. 6. Table 2 lists the cluster information of the two detected sub-regions, including the anatomical locations, cluster size, peak coordinates and spearman correlation coefficient. The detected sub-regions were relatively stable by using the two different M models (DC > 0.85 for each sub-region as listed in Table 2). No sub-regions with increasing $f$$CMRO_2$ with age were detected. As shown in the scatter plots of Fig. 7, the BOLD and OEF signal extracted from the 2 clusters of sub-regional analyses showed no significant changes with age, while both $CMRO_2$ and CBF in the two sub-regions significantly decreased with age. In addition, the associations of CBF and $CMRO_2$ signal changes with age remain significant in two sub-regions upon the inclusion of behavioral performance and GM volume as covariates while BOLD and OEF show no significant trends (see supplement Fig. S3).

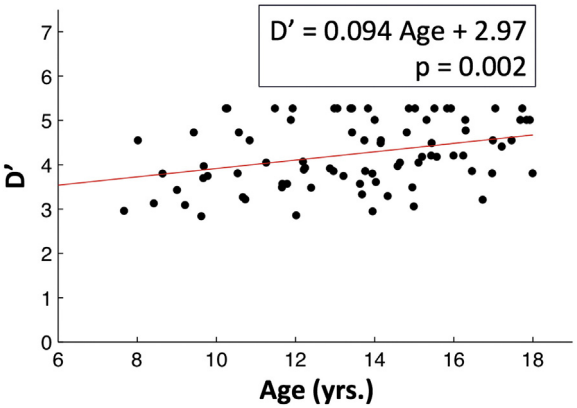

Fig. 3. Behavioral performance (D-prime) of all subjects as a function of age.

4. Discussion

The central theme of the present study was to investigate functional brain development through in vivo assessments of CBF, OEF and $CMRO_2$ both at baseline and during the performance of a working memory task in a cohort of typically developing children aged 7 to 18 years. Using a suite of 4 emerging MRI technologies including MR blood oximetry, PC MRI, pCASL perfusion MRI and concurrent CBF/BOLD fMRI, we have made two main discoveries: 1) At baseline, both global CBF and $CMRO_2$ showed an age related decline while global OEF was stable across the age group; 2) During the performance of a verbal working memory task, neither BOLD nor CBF responses showed significant variations with age in the activated fronto-parietal brain regions. However, detailed voxel-wise analyses revealed sub-regions within the activated fronto-parietal regions that show significant decline of fractional $CMRO_2$ changes with age.

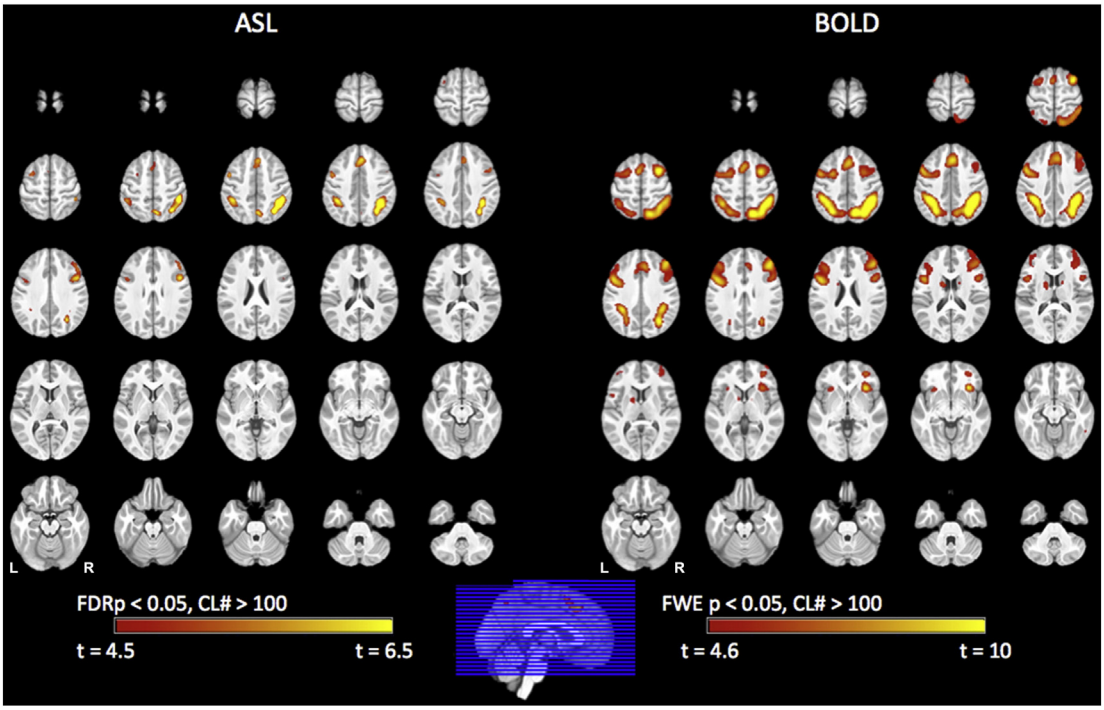

Fig. 4. Group-level activation maps of 2-back vs. 0-back contrast from ASL (left) and BOLD (right) data. Reliable activations can be observed in bilateral prefrontal, parietal cortex and anterior cingulate cortex (ACC) in BOLD and ASL data. Compared to ASL, BOLD shows stronger task-induced brain activation. CBF and BOLD data were thresholded at FDR and FWE corrected $p < 0.05$ with cluster size >100, respectively.

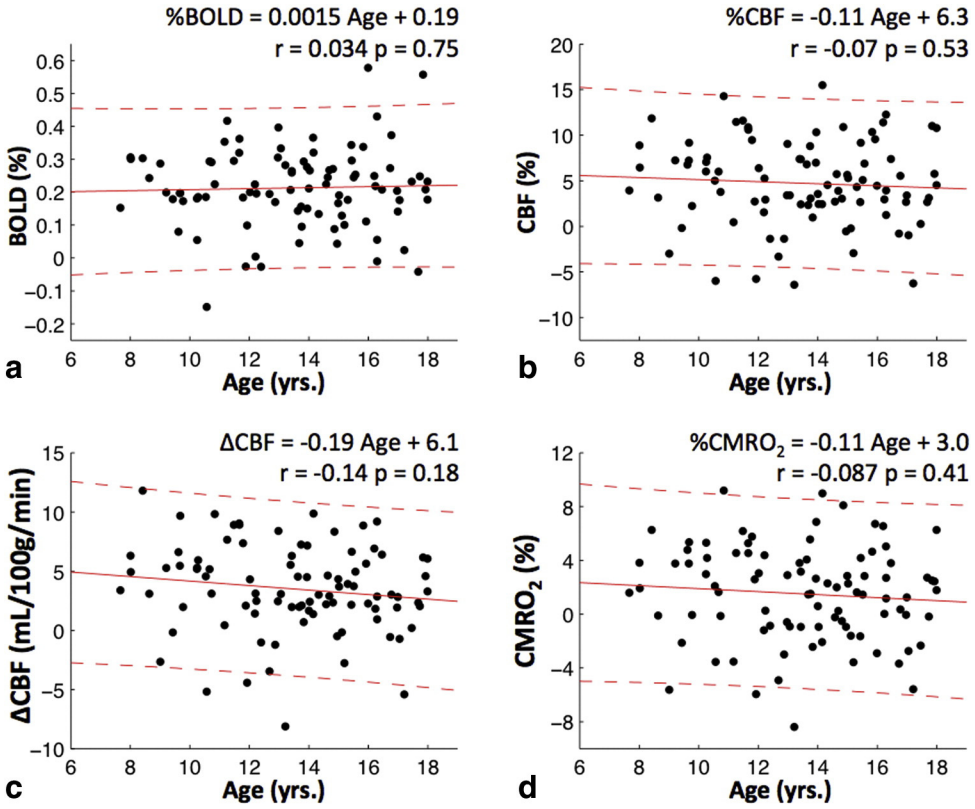

Fig. 5. Scatter plots of task-induced mean BOLD change (a), relative CBF change (b), absolute CBF change (c), and relative $CMRO_2$ change (d) within the combined ROI as a function of age, respectively. Constant $M = 0.07$ was used for the estimation of relative $CMRO_2$ change. Dashed lines indicate 95% confidence interval.

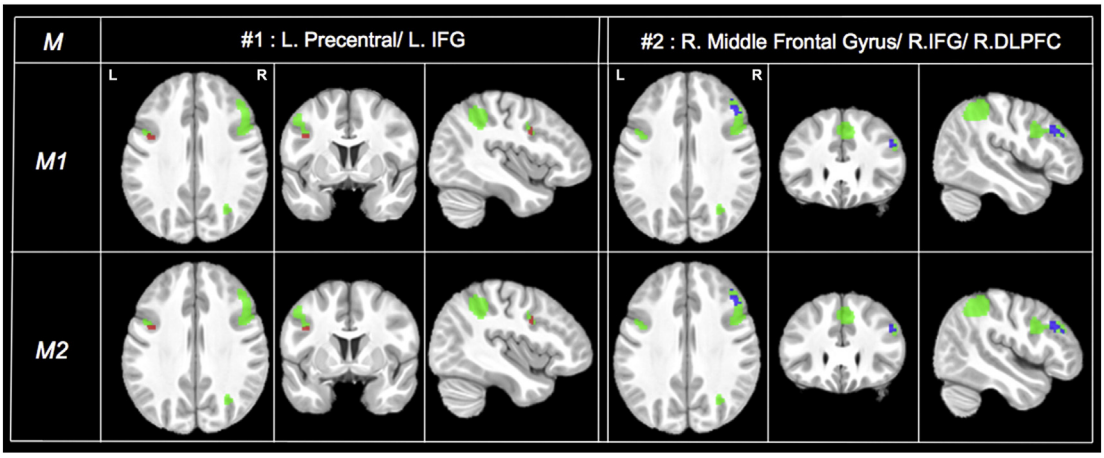

Fig. 6. Sub-regions (#1, and 2) were shown in axial, coronal and sagittal views where the percentage of $CMRO_2$ change was observed to significantly decrease with age using the two M models in red and blue colors, respectively. The conjunction ROI mask from the group-level BOLD and CBF activation maps is shown in green color.

4.1. Developmental trajectories of CBF and $CMRO_2$ at baseline

During the past few decades, template-based structural analyses of pediatric MRI have revealed neurodevelopmental trends of gray and white matter (Gogtay et al., 2004). However, much less is known regarding developmental changes in metrics of function and metabolism of a pediatric brain, such as CBF, cerebral metabolic rate of glucose (CMRglu) and $CMRO_2$. These functional and metabolic parameters provide surrogate markers of brain's energy expenditure and neuronal processes, thereby may be more closely related to the maturation of human behavior compared to brain structural measurements. To date, however, only a handful of nuclear medicine studies (Chiron et al., 1992; Chugani, 1998; Takahashi et al., 1999; Wintermark et al., 2004) reported developmental changes in CBF, CMRglu and $CMRO_2$, suggesting a general peak around 5–8 years followed by tapering to adult levels throughout adolescence. Similar developmental trajectories of resting CBF have recently been shown by ASL perfusion MRI studies (Avants et al., 2015; Biagi et al., 2007; Satterthwaite et al., 2014; Taki et al., 2011a, 2011b; Wang and Licht, 2006; Wang et al., 2003). Detailed region and sex specific developmental trajectories of CBF have been revealed after the effect of age-related variations in cortical structure was adjusted (Satterthwaite et al., 2014; Taki et al., 2011a, 2011b). These studies suggest that ASL CBF may provide a valuable imaging marker of both typical and atypical development of brain function (Wang et al., 2009).

In parallel to ASL techniques, noninvasive MR blood oximetry has recently been developed for quantifying global OEF that exploits the intrinsic susceptibility of deoxygenated hemoglobin (Jain et al., 2010) as well as the blood T2 dependence on venous oxygen saturation, both of the superior sagittal sinus (Lu and Ge, 2008). MR oximetry techniques for mapping regional OEF also emerged based on the quantitative BOLD, susceptibility mapping (R2′) and more recently T2 mapping of venous blood techniques (An and Lin, 2000; Bolar et al., 2011; Christen et al., 2012; He and Yablonskiy, 2007). When combined with CBF measurements by PC MRI and ASL, MR oximetry techniques can provide noninvasive quantification of global and regional $CMRO_2$, respectively. In particular, global OEF and $CMRO_2$ measurement has been shown to be fast and reliable, and has shown clinical utility in neonatal imaging (De Vis et al., 2014; Jain et al., 2014; Liu et al., 2014). The developmental trajectories of global CBF, OEF and $CMRO_2$ at baseline observed in the present study are in excellent agreement with existing PET literature on developmental curves of CBF, CMRglu and $CMRO_2$ (Chiron et al., 1992; Chugani, 1998; Takahashi et al., 1999; Wintermark et al., 2004). While CBF, CMRglu and $CMRO_2$ generally follow an inverted U-shaped function with a peak around 5–8 years of age, OEF has been shown to be relatively stable across age groups by a PET study (Takahashi et al., 1999).

Table 2
Details of significant subregions including anatomical locations, cluster size, coordinates and peak correlation coefficients using the two *M* models. The reliability and spatial stability of the detected sub-regions using the two *M* models was assessed using DC, which is also listed.

Significant ($p < 0.05$, Cluster corrected $\alpha < 0.05$) subregions					
Anatomical locations	*M* model	Cluster size	Peak coordinator	Peak value (spearman R)	DC
L. Precentral/L. IFG	*M1*	22	−42 2 30	−0.22956	0.8718
	M2	17	−40 2 30	−0.22577	
R. Middle frontal gyrus/R. IFG/R. DLPFC(9/46)	*M1*	58	46 26 30	−0.29115	0.9375
	M2	55	46 26 32	−0.28495	

Abbreviations: IFG, inferior frontal gyrus; DLPFC, dorsolateral prefrontal cortex.

4.2. Developmental trajectories of CBF and $CMRO_2$ during fMRI of working memory

The second aim of the present study was to investigate the developmental trajectories of CBF, OEF and $CMRO_2$ responses to a working memory task. This is a potentially significant goal as recent advances in neuroenergetics (Belanger et al., 2011) indicate that during task performance, neuronal demand is the principal driver of changes in oxygen consumption whereas the metabolic profile of astrocytes remains largely glycolytic. In addition, fractional changes in $CMRO_2$ have been found to equal measured fractional changes in neuronal firing rate during forepaw stimulation in rats (Hyder et al., 2002; Maandag et al., 2007).

To date, BOLD fMRI has been the primary neuroimaging tool for studying neurodevelopmental changes. While popular, the BOLD contrast has several limitations that impair its interpretation in terms of the underlying neuronal activity. First, BOLD reflects combined effects of changes in CBF, CBV and $CMRO_2$ in response to stimulation; Second, BOLD lacks absolute quantification and can only assess relative changes compared to a "baseline" condition, thereby making it difficult in differentiating developmental trends in BOLD fMRI as changes in activation or baseline states. Finally, the effect size of BOLD signal changes is intrinsically dependent on the strength of neurovascular coupling which may vary across age groups. Consequently, it is not surprising to see contradictive developmental trends of BOLD fMRI reported by different studies (Crone et al., 2006; Tamm et al., 2002; Thomas et al., 1999). In recognizing the limitations of BOLD fMRI, recent studies have employed concurrent CBF/BOLD fMRI to infer the developmental changes in

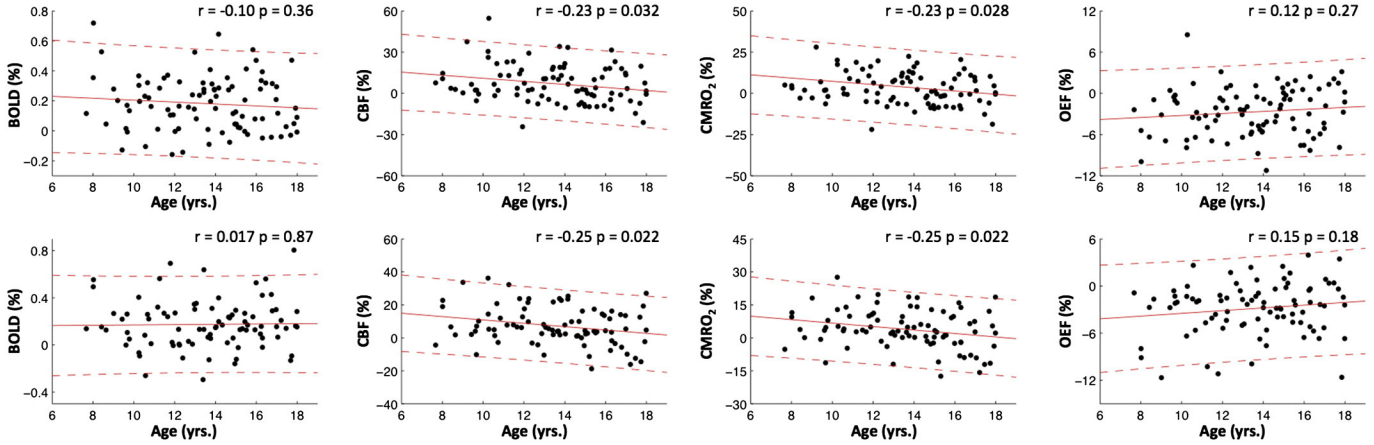

Fig. 7. Scatter plots of BOLD change (a, e), CBF change (b, f), relative $CMRO_2$ change (c, g) and OEF change (d, h) within two sub-regions as a function of age, respectively. Both relative CBF change and $CMRO_2$ change significantly decrease with age in the two sub-regions, while BOLD and OEF changes show no changes with age.

oxidative metabolism in response to sensorimotor and language tasks (Moses et al., 2014; Schmithorst et al., 2015). Preliminary evidence indicates that the strength of neurovascular coupling underlying the BOLD effect increases with age and the metabolic processes may be elevated in younger children (Moses et al., 2014; Schmithorst et al., 2015).

The present study builds on and further extends existing developmental studies utilizing concurrent CBF/BOLD fMRI. A verbal working memory task was employed to engage the fronto-parietal executive network that has been well characterized in developmental fMRI studies (Klingberg et al., 2002a, 2002b; Kwon et al., 2002; Thomason et al., 2009). Fractional changes in $CMRO_2$ were derived from CBF and BOLD fMRI data based on the Davis Model. To account for the potential variation of *M* with age, we adopted two models by incorporating resting global CBF, OEF and $CMRO_2$ data acquired in the present study and literature values of *Hct*. Using both models of *M*, we observed that the average fractional signal changes of CBF, OEF and $CMRO_2$ did not vary significantly with age in the commonly activated fronto-parietal regions in CBF and BOLD fMRI. These findings are in good agreement with two recent CBF/BOLD fMRI studies using sensorimotor and language tasks (Moses et al., 2014; Schmithorst et al., 2015) that showed similar percentage changes of CBF and BOLD signal, yet reduced absolute CBF changes in younger compared to older children.

Our findings of decreasing global CBF and $CMRO_2$ at baseline with age and no regional age variations in relative CBF and $CMRO_2$ changes suggest that the brain's oxidative metabolism and CBF are elevated in younger children both at baseline and in response to working memory tasks. The observations were consistent even with adjustment of potential variations in the strength of neurovascular coupling (different M models), suggesting that in layman's terms, the brain becomes more "energy efficient" with age during development (Haier et al., 1988).

Despite the absence of significant trends in fractional changes in average BOLD, CBF and $CMRO_2$ in the fronto-parietal ROIs, we noticed that the overall correlation coefficients between CBF, $CMRO_2$ changes with age are negative in Fig. 5. Given the ROIs reflect hemodynamic activation and $CMRO_2$ is closely related to neuronal activities, we set out to explore the possibility that there are sub-regions or hubs within the fronto-parietal ROIs demonstrating significant $fCMRO_2$ variations with age. Indeed, voxel-wise regression analyses consistently revealed significant sub-regions with decreasing $fCMRO_2$ with age using two models of *M*. In contrast, no positive associations between $fCMRO_2$ and age were detected. This observation is consistent with the notion that neuronal activation (measured by *f*CMRO2 in our experiment) is more focal while the ensuing hemodynamic responses are more diffuse in space and time.

Another potential explanation of $fCMRO_2$ decreases with age in sub-regions of the fronto-parietal network may be related to the two independent systems implicated in the maintenance of verbal information in working memory, as reviewed by (Camos and Barrouillet, 2014). These two independent systems underlie the attentional refreshing (linked with the dorsolateral PFC) and subvocal rehearsal processing (linked with the ventro lateral PFC) (Raye et al., 2002). The observed reduced $fCMRO_2$ with age in 2 subregions within the left Precentral/IFG and the right MFG/IFG/DLPFC is consistent with the attentional refreshing and the subvocal rehearsal network.

Past studies and the present study show that the performance of the verbal working memory task improves with age (Conklin et al., 2007; Cromer et al., 2015). In the present study, the trend of decreasing $fCMRO_2$ with age remained in the 2 sub-regions when the regression analyses were performed with GM volume and behavioral performance (D′) included as covariates (see supplement Fig. S3). This suggests that our observation of decreasing $fCMRO_2$ with age in the 2 sub-regions is robust and cannot be explained by improving performance or decreasing GM volume with age in this typically developing cohort.

4.3. Limitations and future directions

Previous studies have employed concurrently acquired BOLD and ASL signals to infer the underlying metabolic events and neuronal activity in response to task activation (Gauthier et al., 2013). Such an approach, commonly known as quantitative or calibrated fMRI, generally employs a hypercapnia experiment to calibrate the BOLD effect and determine the fractional change in $CMRO_2$ with activation, assuming that hypercapnia does not alter $CMRO_2$ (Chen and Pike, 2010). Hypercapnia experiment, however, is not feasible or very challenging to be carried out in the pediatric population. Therefore, we employed two models of *M* variations with age which yielded consistent findings of $CMRO_2$ responses to working memory tasks. The SNR of the DE-EPI pCASL scans was relatively low and may contribute to the weak developmental trends of decreasing fractional $CMRO_2$ changes with age in the sub-regional analysis. Our findings of developmental changes of CBF and $CMRO_2$ at baseline and during working memory tasks need to be replicated in future studies.

5. Conclusion

Using a suite of MRI techniques for in vivo assessments of CBF, OEF and $CMRO_2$, we found an age related decline of global CBF and $CMRO_2$ while global OEF was stable in a cohort of children aged 7 to 18 years. In contrast, age related decline of fractional CBF and $CMRO_2$ changes during the performance of a working memory task was more subtle and only detected through sub-regional analyses within the activated fronto-parietal regions. These findings lead to intriguing hypotheses

regarding the developmental trajectories of brain function and neuronal activity to be tested in future studies.

Acknowledgments

The present study was supported by NIH grant R01-MH080892. The authors thank Dr. Hengyi Rao for providing the stimulus program for the working memory task.

Appendix A. Supplementary data

Supplementary data to this article can be found online at http://dx.doi.org/10.1016/j.neuroimage.2016.04.035.

References

An, H., Lin, W., 2000. Quantitative measurements of cerebral blood oxygen saturation using magnetic resonance imaging. J. Cereb. Blood Flow Metab. 20, 1225–1236.
Avants, B.B., Duda, J.T., Kilroy, E., Krasileva, K., Jann, K., Kandel, B.T., Yan, L., Jog, M.A., Smith, R.X., Wang, Y., Dapretto, M., Wang, D.J., 2015. The pediatric template of brain perfusion. Scientific Data 2, 150003.
Belanger, M., Allaman, I., Magistretti, P.J., 2011. Brain energy metabolism: focus on astrocyte-neuron metabolic cooperation. Cell Metab. 14, 724–738.
Biagi, L., Abbruzzese, A., Bianchi, M.C., Alsop, D.C., Del Guerra, A., Tosetti, M., 2007. Age dependence of cerebral perfusion assessed by magnetic resonance continuous arterial spin labeling. J. Magn. Reson. Imaging 25, 696–702.
Bolar, D.S., Rosen, B.R., Sorensen, A.G., Adalsteinsson, E., 2011. QUantitative imaging of eXtraction of oxygen and TIssue consumption (QUIXOTIC) using venular-targeted velocity-selective spin labeling. Magn. Reson. Med. 66, 1550–1562.
Camos, V., Barrouillet, P., 2014. Attentional and non-attentional systems in the maintenance of verbal information in working memory: the executive and phonological loops. Front. Hum. Neurosci. 8, 900.
Casey, B.J., Tottenham, N., Liston, C., Durston, S., 2005. Imaging the developing brain: what have we learned about cognitive development? Trends Cogn. Sci. 9, 104–110.
Chen, J.J., Pike, G.B., 2009. BOLD-specific cerebral blood volume and blood flow changes during neuronal activation in humans. NMR Biomed. 22, 1054–1062.
Chen, J.J., Pike, G.B., 2010. Global cerebral oxidative metabolism during hypercapnia and hypocapnia in humans: implications for BOLD fMRI. J. Cereb. Blood Flow Metab. 30, 1094–1099.
Chen, J., Jann, K., Wang, D.J., 2015. Characterizing resting-state brain function using arterial-spin labeling. Brain Connect.
Chiron, C., Raynaud, C., Maziere, B., Zilbovicius, M., Laflamme, L., Masure, M.C., Dulac, O., Bourguignon, M., Syrota, A., 1992. Changes in regional cerebral blood flow during brain maturation in children and adolescents. J. Nucl. Med. 33, 696–703.
Christen, T., Schmiedeskamp, H., Straka, M., Bammer, R., Zaharchuk, G., 2012. Measuring brain oxygenation in humans using a multiparametric quantitative blood oxygenation level dependent MRI approach. Magn. Reson. Med. 68, 905–911.
Chugani, H.T., 1998. A critical period of brain development: studies of cerebral glucose utilization with PET. Prev. Med. 27, 184–188.
Conklin, H.M., Luciana, M., Hooper, C.J., Yarger, R.S., 2007. Working memory performance in typically developing children and adolescents: behavioral evidence of protracted frontal lobe development. Dev. Neuropsychol. 31, 103–128.
Cromer, J.A., Schembri, A.J., Harel, B.T., Maruff, P., 2015. The nature and rate of cognitive maturation from late childhood to adulthood. Front. Psychol. 6, 704.
Crone, E.A., Wendelken, C., Donohue, S., van Leijenhorst, L., Bunge, S.A., 2006. Neurocognitive development of the ability to manipulate information in working memory. Proc. Natl. Acad. Sci. U. S. A. 103, 9315–9320.
Davis, T.L., Kwong, K.K., Weisskoff, R.M., Rosen, B.R., 1998. Calibrated functional MRI: mapping the dynamics of oxidative metabolism. Proc. Natl. Acad. Sci. U. S. A. 95, 1834–1839.
De Vis, J.B., Petersen, E.T., Alderliesten, T., Groenendaal, F., de Vries, L.S., van Bel, F., Benders, M.J., Hendrikse, J., 2014. Non-invasive MRI measurements of venous oxygenation, oxygen extraction fraction and oxygen consumption in neonates. NeuroImage 95, 185–192.
Gauthier, C.J., Madjar, C., Desjardins-Crepeau, L., Bellec, P., Bherer, L., Hoge, R.D., 2013. Age dependence of hemodynamic response characteristics in human functional magnetic resonance imaging. Neurobiol. Aging 34, 1469–1485.
Giedd, J.N., Blumenthal, J., Jeffries, N.O., Castellanos, F.X., Liu, H., Zijdenbos, A., Paus, T., Evans, A.C., Rapoport, J.L., 1999. Brain development during childhood and adolescence: a longitudinal MRI study. Nat. Neurosci. 2, 861–863.
Gogtay, N., Giedd, J.N., Lusk, L., Hayashi, K.M., Greenstein, D., Vaituzis, A.C., Nugent 3rd, T.F., Herman, D.H., Clasen, L.S., Toga, A.W., Rapoport, J.L., Thompson, P.M., 2004. Dynamic mapping of human cortical development during childhood through early adulthood. Proc. Natl. Acad. Sci. U. S. A. 101, 8174–8179.
Haier, R.J., Siegel, B.V., Nuechterlein, K.H., Hazlett, E., Wu, J.C., Paek, J., Browning, H.L., Buchsbaum, M.S., 1988. Cortical glucose metabolic rate correlates of abstract reasoning and attention studied with positron emission tomography. Intelligence 12, 199–217.
Harris, J.J., Reynell, C., Attwell, D., 2011. The physiology of developmental changes in BOLD functional imaging signals. Dev. Cogn. Neurosci. 1, 199–216.
He, X., Yablonskiy, D.A., 2007. Quantitative BOLD: mapping of human cerebral deoxygenated blood volume and oxygen extraction fraction: default state. Magn. Reson. Med. 57, 115–126.
Hoge, R.D., Atkinson, J., Gill, B., Crelier, G.R., Marrett, S., Pike, G.B., 1999. Investigation of BOLD signal dependence on cerebral blood flow and oxygen consumption: the deoxyhemoglobin dilution model. Magn. Reson. Med. 42, 849–863.
Hyder, F., Rothman, D.L., Shulman, R.G., 2002. Total neuroenergetics support localized brain activity: implications for the interpretation of fMRI. Proc. Natl. Acad. Sci. U. S. A. 99, 10771–10776.
Jain, V., Langham, M.C., Wehrli, F.W., 2010. MRI estimation of global brain oxygen consumption rate. J. Cereb. Blood Flow Metab. 30, 1598–1607.
Jain, V., Duda, J., Avants, B., Giannetta, M., Xie, S.X., Roberts, T., Detre, J.A., Hurt, H., Wehrli, F.W., Wang, D.J., 2012. Longitudinal reproducibility and accuracy of pseudo-continuous arterial spin-labeled perfusion MR imaging in typically developing children. Radiology 263, 527–536.
Jain, V., Buckley, E.M., Licht, D.J., Lynch, J.M., Schwab, P.J., Naim, M.Y., Lavin, N.A., Nicolson, S.C., Montenegro, L.M., Yodh, A.G., Wehrli, F.W., 2014. Cerebral oxygen metabolism in neonates with congenital heart disease quantified by MRI and optics. J. Cereb. Blood Flow Metab. 34, 380–388 official journal of the International Society of Cerebral Blood Flow and Metabolism.
Klingberg, T., Forssberg, H., Westerberg, H., 2002a. Increased brain activity in frontal and parietal cortex underlies the development of visuospatial working memory capacity during childhood. J. Cogn. Neurosci. 14, 1–10.
Klingberg, T., Forssberg, H., Westerberg, H., 2002b. Training of working memory in children with ADHD. J. Clin. Exp. Neuropsychol. 24, 781–791.
Kwon, H., Reiss, A.L., Menon, V., 2002. Neural basis of protracted developmental changes in visuo-spatial working memory. Proc. Natl. Acad. Sci. U. S. A. 99, 13336–13341.
Kwong, K.K., Belliveau, J.W., Chesler, D.A., Goldberg, I.E., Weisskoff, R.M., Poncelet, B.P., Kennedy, D.N., Hoppel, B.E., Cohen, M.S., Turner, R., et al., 1992. Dynamic magnetic resonance imaging of human brain activity during primary sensory stimulation. Proc. Natl. Acad. Sci. U. S. A. 89, 5675–5679.
Leithner, C., Royl, G., 2014. The oxygen paradox of neurovascular coupling. J. Cereb. Blood Flow Metab. 34, 19–29.
Lenroot, R.K., Giedd, J.N., 2006. Brain development in children and adolescents: insights from anatomical magnetic resonance imaging. Neurosci. Biobehav. Rev. 30, 718–729.
Liu, P., Huang, H., Rollins, N., Chalak, L.F., Jeon, T., Halovanic, C., Lu, H., 2014. Quantitative assessment of global cerebral metabolic rate of oxygen (CMRO2) in neonates using MRI. NMR Biomed. 27, 332–340.
Lu, H., Ge, Y., 2008. Quantitative evaluation of oxygenation in venous vessels using T2-relaxation-under-spin-tagging MRI. Magn. Reson. Med. 60, 357–363 official journal of the Society of Magnetic Resonance in Medicine/Society of Magnetic Resonance in Medicine.
Lu, H., Hutchison, J., Xu, F., Rypma, B., 2011. The relationship between M in "calibrated fMRI" and the physiologic modulators of fMRI. Open Neuroimaging J. 5, 112–119.
Maandag, N.J., Coman, D., Sanganahalli, B.G., Herman, P., Smith, A.J., Blumenfeld, H., Shulman, R.G., Hyder, F., 2007. Energetics of neuronal signaling and fMRI activity. Proc. Natl. Acad. Sci. U. S. A. 104, 20546–20551.
Moses, P., DiNino, M., Hernandez, L., Liu, T.T., 2014. Developmental changes in resting and functional cerebral blood flow and their relationship to the BOLD response. Hum. Brain Mapp. 35, 3188–3198.
Ogawa, S., Lee, T.M., Kay, A.R., Tank, D.W., 1990. Brain magnetic resonance imaging with contrast dependent on blood oxygenation. Proc. Natl. Acad. Sci. U. S. A. 87, 9868–9872.
Paus, T., 2005. Mapping brain maturation and cognitive development during adolescence. Trends Cogn. Sci. 9, 60–68.
Power, J.D., Barnes, K.A., Snyder, A.Z., Schlaggar, B.L., Petersen, S.E., 2012. Spurious but systematic correlations in functional connectivity MRI networks arise from subject motion. NeuroImage 59, 2142–2154.
Raye, C.L., Johnson, M.K., Mitchell, K.J., Reeder, J.A., Greene, E.J., 2002. Neuroimaging a single thought: dorsolateral PFC activity associated with refreshing just-activated information. NeuroImage 15, 447–453.
Satterthwaite, T.D., Shinohara, R.T., Wolf, D.H., Hopson, R.D., Elliott, M.A., Vandekar, S.N., Ruparel, K., Calkins, M.E., Roalf, D.R., Gennatas, E.D., Jackson, C., Erus, G., Prabhakaran, K., Davatzikos, C., Detre, J.A., Hakonarson, H., Gur, R.C., Gur, R.E., 2014. Impact of puberty on the evolution of cerebral perfusion during adolescence. Proc. Natl. Acad. Sci. U. S. A. 111, 8643–8648.
Schmithorst, V.J., Vannest, J., Lee, G., Hernandez-Garcia, L., Plante, E., Rajagopal, A., Holland, S.K., 2015. Evidence that neurovascular coupling underlying the BOLD effect increases with age during childhood. Hum. Brain Mapp. 36, 1–15.
Song, X.W., Dong, Z.Y., Long, X.Y., Li, S.F., Zuo, X.N., Zhu, C.Z., He, Y., Yan, C.G., Zang, Y.F., 2011. REST: a toolkit for resting-state functional magnetic resonance imaging data processing. PLoS One 6, e25031.
Szaflarski, J.P., Altaye, M., Rajagopal, A., Eaton, K., Meng, X., Plante, E., Holland, S.K., 2012. A 10-year longitudinal fMRI study of narrative comprehension in children and adolescents. NeuroImage 63, 1188–1195.
Takahashi, T., Shirane, R., Sato, S., Yoshimoto, T., 1999. Developmental changes of cerebral blood flow and oxygen metabolism in children. AJNR Am. J. Neuroradiol. 20, 917–922.
Taki, Y., Hashizume, H., Sassa, Y., Takeuchi, H., Wu, K., Asano, M., Asano, K., Fukuda, H., Kawashima, R., 2011a. Correlation between gray matter density-adjusted brain perfusion and age using brain MR images of 202 healthy children. Hum. Brain Mapp. 32, 1973–1985.
Taki, Y., Hashizume, H., Sassa, Y., Takeuchi, H., Wu, K., Asano, M., Asano, K., Fukuda, H., Kawashima, R., 2011b. Gender differences in partial-volume corrected brain perfusion using brain MRI in healthy children. NeuroImage 58, 709–715.

Tamm, L., Menon, V., Reiss, A.L., 2002. Maturation of brain function associated with response inhibition. J. Am. Acad. Child Adolesc. Psychiatry 41, 1231–1238.
Thomas, K.M., King, S.W., Franzen, P.L., Welsh, T.F., Berkowitz, A.L., Noll, D.C., Birmaher, V., Casey, B.J., 1999. A developmental functional MRI study of spatial working memory. NeuroImage 10, 327–338.
Thomason, M.E., Race, E., Burrows, B., Whitfield-Gabrieli, S., Glover, G.H., Gabrieli, J.D., 2009. Development of spatial and verbal working memory capacity in the human brain. J. Cogn. Neurosci. 21, 316–332.
Wang, J., Licht, D.J., 2006. Pediatric perfusion MRI with arterial spin labeling. Neuroimaging Clin. N. Am. 16, 149–167.
Wang, J., Licht, D.J., Jahng, G.H., Liu, C.S., Rabin, J.T., Haselgrove, J.C., Zimmerman, R.A., Detre, J.A., 2003. Pediatric perfusion imaging using pulsed arterial spin labeling. J. Magn. Reson. Imaging 18, 404–413.
Wang, J., Rao, H., Detre, J.A., 2009. Arterial spin labeling perfusion MRI in developmental neuroscience. In: Rumsey, J.M., Ernst, M. (Eds.), Neuroimging in Developmental Clinical Neuroscience. Cambridge University Press, Cambridge, pp. 326–343.
Wickens, T.D., 2001. Elementary Signal Detection Theory. OUP USA, p. 20.
Wintermark, M., Lepori, D., Cotting, J., Roulet, E., van Melle, G., Meuli, R., Maeder, P., Regli, L., Verdun, F.R., Deonna, T., Schnyder, P., Gudinchet, F., 2004. Brain perfusion in children: evolution with age assessed by quantitative perfusion computed tomography. Pediatrics 113, 1642–1652.
Wu, W.C., Jain, V., Li, C., Giannetta, M., Hurt, H., Wehrli, F.W., Wang, D.J., 2010. In vivo venous blood T(1) measurement using inversion recovery true-FISP in children and adults. Magn. Reson. Med. 64, 1140–1147.